Trapped electron damping of geodesic acoustic mode

H. S. Zhang[1,2] and Z. Lin[2,a)]
[1]*Fusion Simulation Center and State Key Laboratory of Nuclear Physics and Technology, Peking University, Beijing 100871, China*
[2]*Department of Physics and Astronomy, University of California, Irvine, California 92697, USA*

(Received 2 March 2010; accepted 13 May 2010; published online 15 July 2010)

Global gyrokinetic particle simulation finds that the collisionless damping rate of the geodesic acoustic mode (GAM) in tokamak is greatly enhanced by trapped electrons in the high-q region of tokamak (q is the safety factor). The electron damping has been identified to arise from the resonance of the GAM oscillation with the trapped electron bounce motion. The contribution of passing electrons to the GAM collisionless damping is much smaller than the trapped electrons. The residual level of the zonal flow is not sensitive to the trapped electron resonance. © *2010 American Institute of Physics*. [doi:10.1063/1.3447879]

I. INTRODUCTION

Geodesic acoustic mode[1] (GAM) and zonal flow[2] have been widely observed in tokamak experiments.[3–8] Both of them are electrostatic modes that can be spontaneously generated by turbulence and, in return, regulate turbulence.[9,10] Different from the zonal flow, which is zero frequency and can only be damped by collisions, GAM has a finite frequency of the order of ion transit frequency and can be damped through collisionless wave-particle resonance, i.e., ion Landau damping, in the small-q region.[11,12] As the safety factor q increases, the ion transit frequency $\omega_t=v_i/(qR_0)$ (v_i is the ion thermal speed and R_0 is the tokamak major radius) becomes much smaller than the GAM frequency, and the damping rate through the primary resonance is reduced. On the other hand, the finite orbit width effect can lead to higher order resonance for short wavelength GAM in the high-q region.[13–15] Moreover, the GAM with short radial wavelength can convert to kinetic GAM and propagate in the radial direction.[16] In addition to turbulence excitation,[10,17] GAM can also be excited by the velocity anisotropy of energetic particles (EGAM).[18] Regarding the nonlinear physics, the GAM second harmonic is recently observed in tokamak experiments.[19,20] The generation of the second harmonic represents an energy sink for the primary GAM oscillation.[21] The GAM nonlinear self-interaction has been studied using fluid theory, but with conflicting results.[22–24] Meanwhile, the gyrokinetic theory and simulation find that the nonlinear self-interaction of the GAM cannot efficiently generate the second harmonic due to a cancellation between the perpendicular convective nonlinearity and the parallel nonlinearity.[25]

Linear GAM properties have been intensively studied through simulations and theory.[13–15,26–28] Because the electron transit frequency is much larger than the GAM frequency, electrons were conjectured to play little roles in the GAM collisionless damping. Therefore, previous works on the GAM collisionless damping usually assume that the electron response is adiabatic. However, the frequency of the trapped electron bounce motion and low energy passing electron transit motion could be close to the GAM frequency in the high-q region where the ion damping effect is weak. Thus the kinetic electron effect should also be considered in the GAM collisionless damping.

In this work, we use the gyrokinetic toroidal code[9,29] (GTC) to study the collisionless GAM properties with kinetic electrons. In our simulation, an initial zonal flow undergoes a damped GAM oscillation and eventually reaches a residual level in the long time collisionless process.[30,31] The residual level of the zonal flow in the simulation agrees well with the theory.[30,32] The frequency and damping rate of the GAM oscillation also correspond to the analytic results in the adiabatic electron response. We calculate in detail the GAM collisionless damping rate in the inverse aspect ratio ϵ and $k_r\rho_i$ scan (k_r is the radial wavevector of GAM and ρ_i is the ion Larmor radius). Finally, we investigate the kinetic electron response in the GAM collisionless damping process. We find that the residual level of the zonal flow changes little but the GAM damping rate is greatly enhanced by the trapped

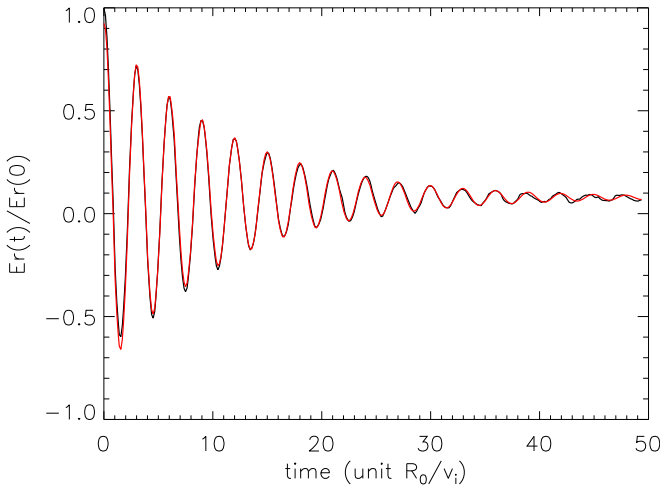

FIG. 1. (Color online) Time evolution of the radial electric field from the simulation with $\epsilon=0.05$ and $q=1.2$ (black) and from the numerical fitting (gray or red online).

a)Author to whom correspondence should be addressed. Electronic mail: zhihongl@uci.edu.

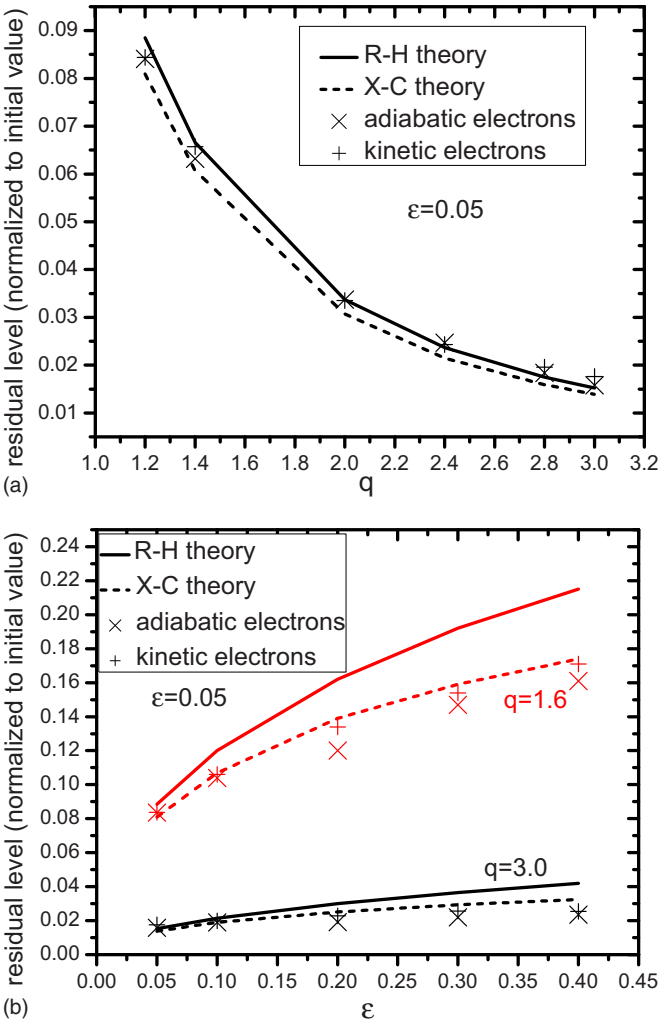

FIG. 2. (Color online) Residual level of the zonal flow with adiabatic and kinetic electrons. (a) is a q scan at $\epsilon=0.05$, while (b) is an ϵ scan at $q=1.6$ (gray or red online) and $q=3.0$ (black).

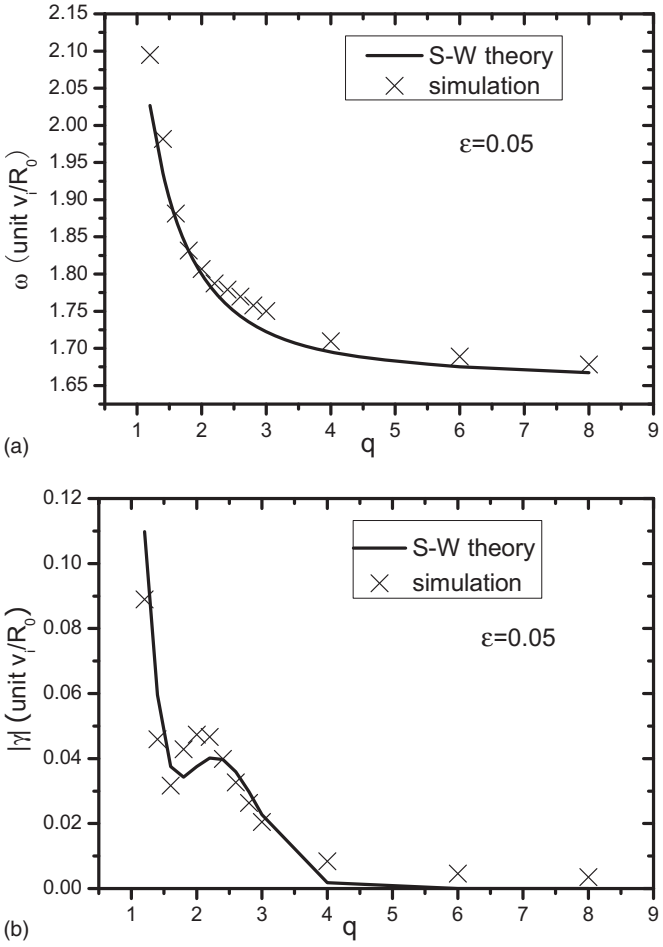

FIG. 3. Results of simulations with adiabatic electrons for the GAM frequency (a) and collisionless damping rate (b) and comparison with S-W theory.

electrons through a resonance of the bounce motion with the GAM oscillation. The passing electron contribution is much smaller than the trapped electrons on the GAM collisionless damping. The electron resonance is clearly verified by the structure of the perturbed electron distribution function in the phase space.

The paper is organized as follows. The effect of kinetic electrons in the zonal flow residual level is discussed in Sec. II. In Sec. III, the effect of kinetic electrons in the GAM collisionless damping is investigated. Section IV is the conclusion and discussion.

II. EFFECT OF KINETIC ELECTRONS IN ZONAL FLOW RESIDUAL LEVEL

In our GTC particle simulations, a flux-surface-averaged ion guiding center density perturbation is initiated to generate the zonal flow. The radial profile of the zonal flow is set to be a sin function with the wavevector to be $k_r\rho_i=0.11$. Also the density perturbation at the inner and outer boundaries is initiated to be zero. We use a small simulation domain $\Delta r=[0.45a, 0.55a]$ (a is the minor radius), $T_i=T_e$, and a constant q profile as the magnetic shear has little effect on the GAM damping and zonal flow residual. We use the particle velocity pitch $P=v_\perp/v$ at $\theta=0$ poloidal midplane to define the simulation boundary of kinetic electrons, i.e., electrons with $P>\sqrt{(1-\epsilon)/(1+\epsilon)}$ are treated as kinetic electrons, while other electrons are treated as adiabatic electrons. An electrostatic version of the fluid-kinetic hybrid electron model[33,34] is used to treat the kinetic electron response in our simulations. Figure 1 is the time evolution of the radial electric field (E_r) of the zonal flow in GTC simulation with adiabatic electron. The following equation is used to fit the simulation result:[12]

$$E_r(t) = A_1 e^{-\gamma t}\cos(\omega_{\mathrm{GAM}} t + \alpha) + A_2. \quad (1)$$

Here ω_{GAM} is the real frequency and γ is the damping rate of the GAM. α is the initial phase and A_2 is the residual level of the zonal flow. The numerical fitting result matches the simulation result very well when appropriate values of ω_{GAM}, γ, A_1, and A_2 are chosen. From Fig. 1 we can see that the radial electric field evolves with a finite frequency ω_{GAM} and quickly damped, i.e., the GAM oscillation, and then reaches a steady state A_2, i.e., the residual flow. This residual level is very important to determine the turbulence level in the nonlinear process.

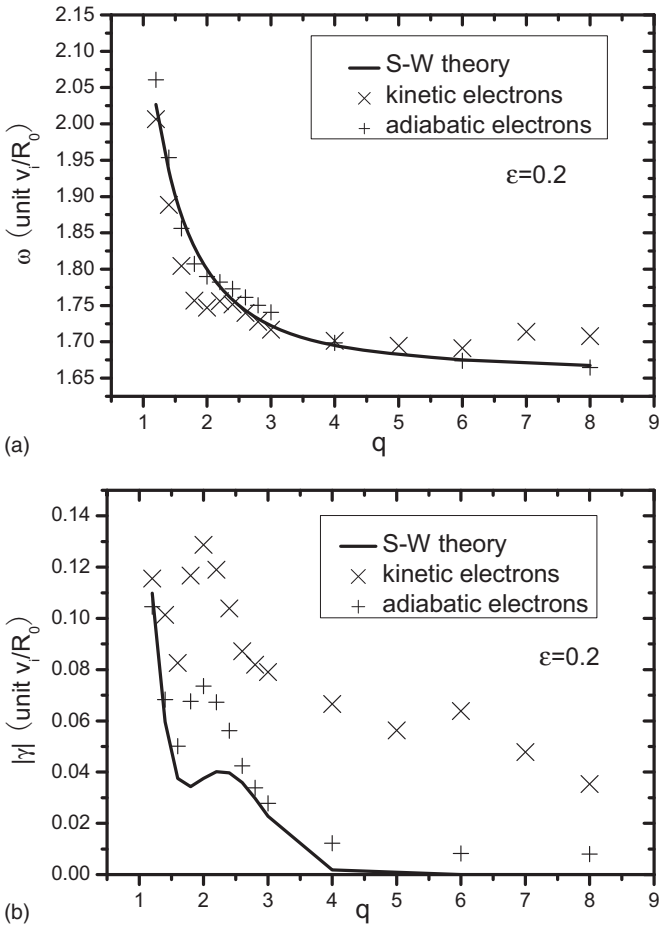

FIG. 4. Comparison of the GAM real frequency and damping rate between adiabatic and kinetic electron simulations at different q.

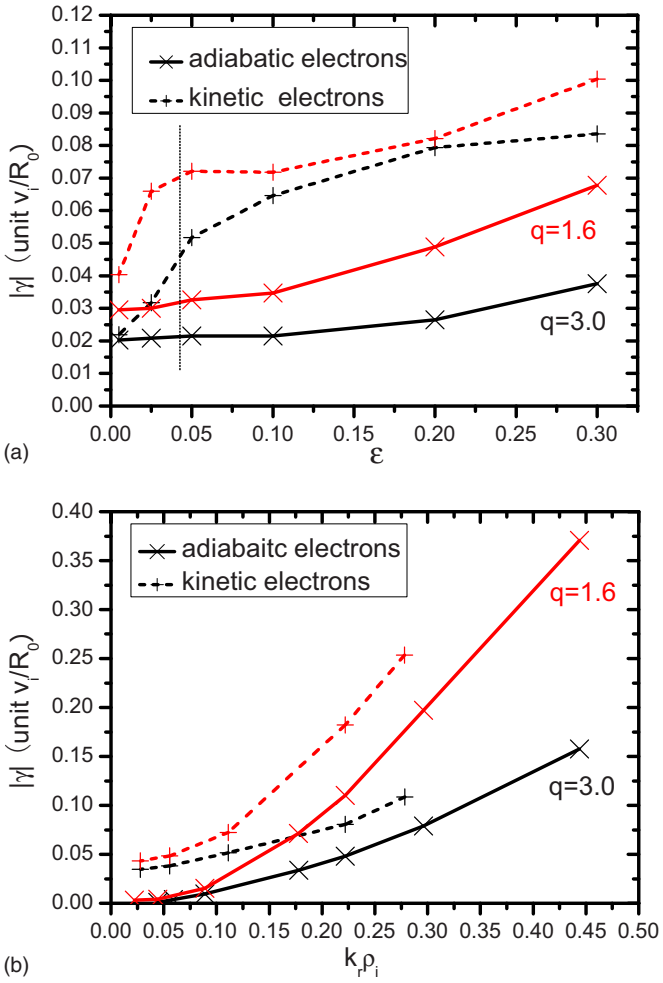

FIG. 5. (Color online) GAM damping rate vs ϵ and $k_r\rho_i$ at $q=1.6$ (gray or red online) and $q=3.0$ (black). The solid lines and the dashed lines are adiabatic electron and kinetic electron simulation, respectively.

The residual level of the zonal flow was calculated by Rosenbluth and Hinton[30] [Rosenblunth–Hinton theory (R-H theory)], by assuming an adiabatic electron response and a small inverse aspect ratio $\epsilon=r/R_0$, with r as the minor radius and R_0 as the major radius,

$$\frac{E_r(t=\infty)}{E_r(t=0)}=\frac{1}{1+1.6q^2/\sqrt{\epsilon}}, \tag{2}$$

where q is the safety factor. An improved calculation was later given by Xiao and Catto[32] [Xiao–Catto theory (X-C theory)] by considering the plasma shaping effects such as elongation and triangularity and finite aspect ratio. For present simulations with circular cross section, the higher order ϵ corrections is given by

$$\frac{E_r(t=\infty)}{E_r(t=0)}=\frac{1}{1+Sq^2/\sqrt{\epsilon}}, \tag{3}$$

$$\text{where}\quad S=\left(3.27+\sqrt{\epsilon}+0.722\epsilon-\frac{0.03}{q^2}\epsilon\right)\Big/2. \tag{4}$$

The zonal flow residual level from GTC simulation and the two theories are compared in Fig. 2. For the circular cross section and a small $\epsilon=0.05$, the differences between the two theoretical residual levels are very small. We can see in Fig. 2(a) that the simulation results of the adiabatic and kinetic electron response are almost the same and agree very well with the theories.

For a larger ϵ, the residual level from the X-C theory is lower than the R-H theory due to the higher order ϵ correction [Fig. 2(b)]. Our simulations reproduce the X-C analytical results. The kinetic electron has very little effects on the residual level of the zonal flow.

III. EFFECT OF KINETIC ELECTRONS IN COLLISIONLESS DAMPING OF GAM

Assuming large aspect ratio ($\epsilon \ll 1$) and adiabatic electron response, the collisionless damping rate of GAM has been calculated by Sugama and Watanabe[15] [Sugama–Watanabe theory (S-W theory)]. The second order resonance for the short wavelength zonal flow is also taken into account. In our GTC simulation, the GAM real frequency and damping rate for $k_r\rho_i=0.11$ are compared to the S-W theory in Fig. 3. From Fig. 3(a) we can see that the simulation frequency agrees very well with the theory within 5% accuracy. When $q \gg 1$, ω_{GAM} becomes a constant as expected. In Fig. 3(b), the GAM damping rate is also shown to correspond well to the theory. The peak around $q=2.2$ is due to

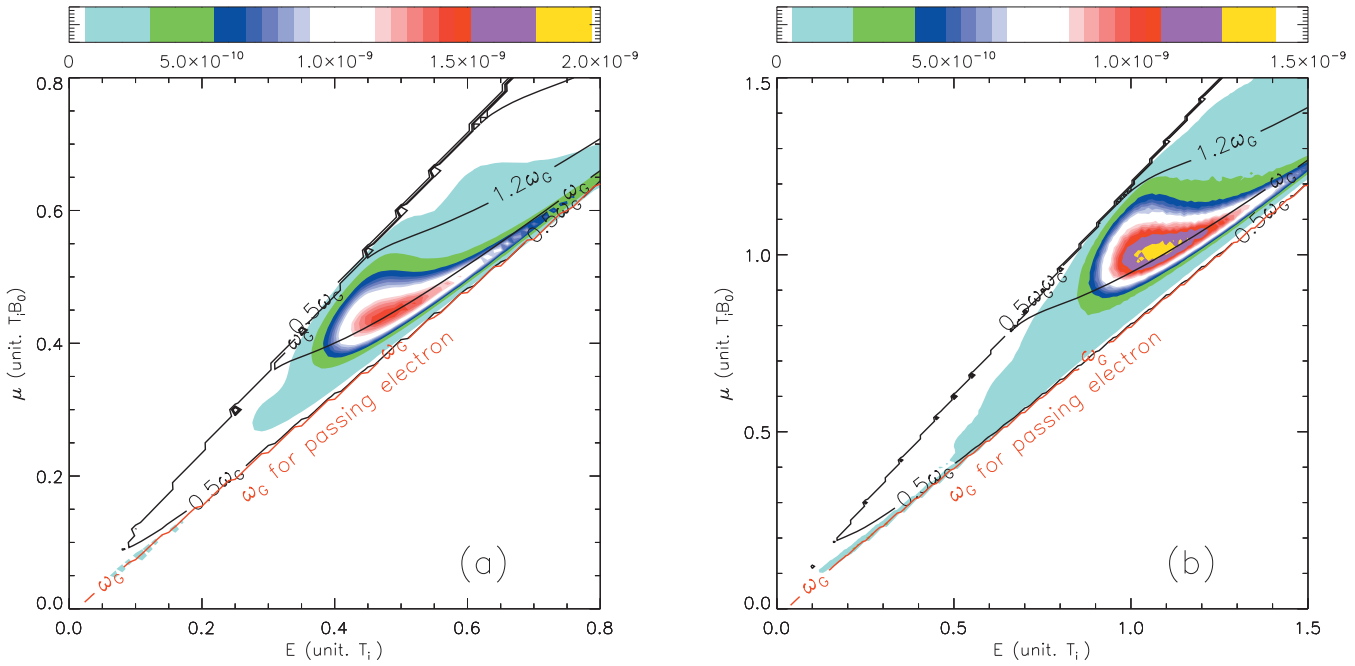

FIG. 6. (Color) Contour plot of trapped electron bounce frequency ω_{be} and passing electron transit frequency ω_{te} (in unit of $\omega_G \equiv \omega_{\mathrm{GAM}}$) along with the simulation result of the $(\delta f_e/f_{e0})^2$ in E-μ space. Here (a) and (b) are simulation with $q=4$ and $q=6$, respectively.

the second order resonance arising from the finite orbit width effect. This effect dominates the collisionless GAM damping at high-q region since the first order GAM damping rate becomes zero when $q>2.0$.[13] When $q \gg 1$, our simulation damping rate does not vanish due to higher order resonances, as shown in a numerical solution[14] or a theory using large $k_r\rho_i q^2$ expansion.[27]

Theoretical derivation of the GAM dispersion relation usually assumes that electrons are adiabatic[14,15] to the $n=0$ mode, i.e., Boltzmann relation for the $m \neq 0$ harmonics but no response to the $m=0$ harmonic. However, trapped electrons could have resonance with the GAM in the high-q region. The trapped electron bounce frequency is $\omega_{be} \approx \sqrt{\epsilon} v_e/(qR_0) \approx (43\sqrt{\epsilon}/q)v_i/R_0$ for hydrogen ions, which is close to the magnitude of the GAM frequency ($\omega_{\mathrm{GAM}} \approx 2.0 v_i/R_0$) for small ϵ and large q. So it is possible that GAM can be damped through resonance with trapped electron bounce motion. Since the number of trapped particles is proportional to $\sqrt{\epsilon}$, $\epsilon=0.2$ is used in the following simulation, comparisons are made between kinetic and adiabatic electron simulations. It is shown that the GAM frequency is insensitive to the trapped electrons while the GAM damping rate is significantly enhanced (Fig. 4).

From Fig. 4(a), the frequency of the simulations with kinetic electrons and $\epsilon=0.2$ is almost the same as simulations with adiabatic electrons and $\epsilon=0.05$ [Fig. 3(a)] except for a small correction at $q \approx 2.0$ and $q \approx 7.0$. As for the damping rate in Fig. 4(b), simulation results with adiabatic electrons at $\epsilon=0.2$ are slightly higher than the theory due to the finite ϵ effects.[13] More importantly, we find that the damping rate in the simulations with kinetic electrons at $\epsilon=0.2$ is much higher than that of adiabatic electrons. We note that when q is larger than 3.0, the results of simulation with kinetic electrons are almost one order of magnitude higher than adiabatic electrons. This means that the trapped electron effect is typically more important than the finite orbit width effect on the GAM damping rate in the high-q region.

In Fig. 5, we plot the GAM damping rate versus ϵ and $k_r\rho_i$ with adiabatic and kinetic electron simulations for $q=3.0$ and $q=1.6$. The real frequency of GAM is not plotted here because it is insensitive to the ϵ and $k_r\rho_i$ in both adiabatic and kinetic electron simulations. In Fig. 5(a), the damping rate increases with ϵ in both adiabatic and kinetic electron simulation cases. When $\epsilon \to 0$, the fraction of trapped electrons decreases to zero, and the simulation results in the kinetic electron cases approach the adiabatic electron cases (left side of the solid line). It is noted that the small ϵ will

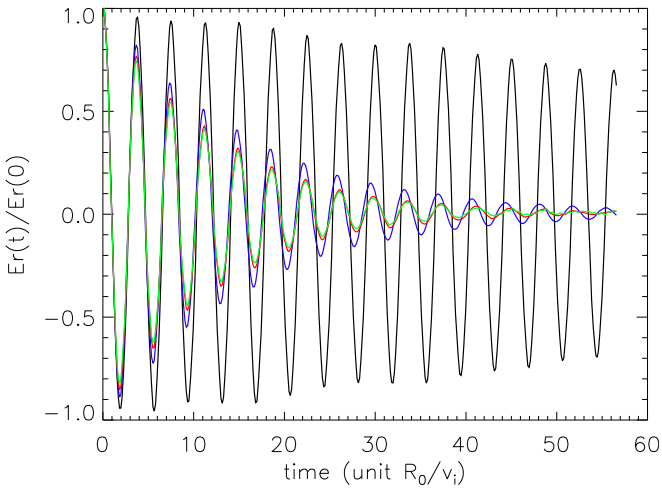

FIG. 7. (Color online) Time evolution of GAM radial electric field for $q=6.0$ and $\epsilon=0.2$. The black line is simulation with adiabatic electrons. The blue, red, and green lines (or gray lines) are kinetic electron simulations with $P=0.82$, 0.71, and 0.59, respectively.

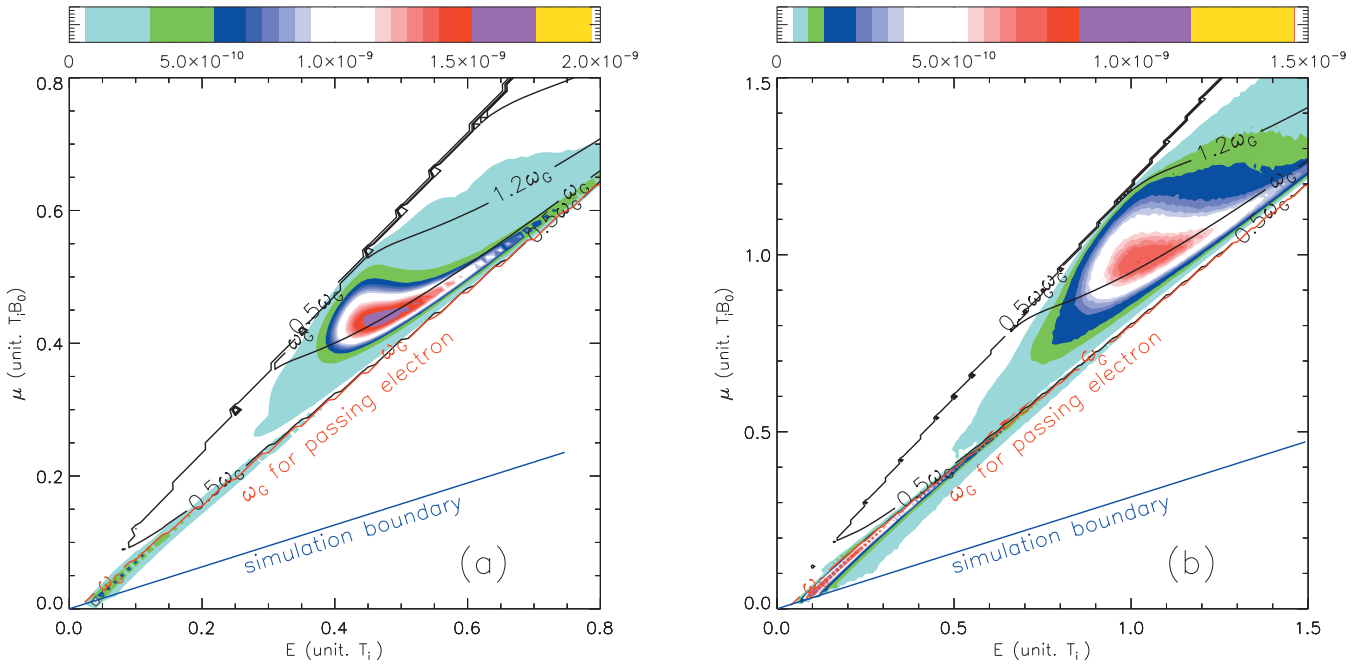

FIG. 8. (Color) Contour plot of ω_{be} and ω_{te} (in unit of $\omega_G \equiv \omega_{\mathrm{GAM}}$) along with the simulation result of the $(\delta f_e/f_{e0})^2$ in E-μ space. Here (a) and (b) are simulation with $q=4$ and $q=6$, respectively. The red line corresponds to $\omega_{te}=\omega_{\mathrm{GAM}}$. The blue line is the kinetic electron boundary for $P=0.59$ in the simulation.

enhance the resonance between GAM and trapped electron bounce motion since $\omega_{be} \propto \sqrt{\epsilon}$, but the number of trapped electrons is also proportional to $\sqrt{\epsilon}$. So the GAM damping rate is not enhanced when $\epsilon \to 0$. When $\epsilon > 0.05$, The trapped electron effect becomes strong, which makes the damping rate of the kinetic electron cases much larger than the adiabatic electron cases (right side of the dot line). In the $k_r\rho_i$ scan of the GAM damping rate [Fig. 5(b)], it is shown that when $k_r\rho_i$ decreases to zero, where the finite orbit width effect disappears, the GAM damping rate of the adiabatic electrons decreases to almost zero but the GAM damping rate of the kinetic electrons still has a finite value due to trapped electron contribution. As $k_r\rho_i$ increases, the finite orbit width effect becomes strong and the damping rate increases rapidly. The damping rate in the kinetic electron cases is higher than the adiabatic electron cases, but the scaling is almost the same. This suggests that the trapped electron and the finite orbit width effects are two independent effects.

In order to further illustrate that the enhancement of the GAM damping rate in the kinetic electron simulation is mainly due to the trapped electron response, we analyze the $(\delta f_e/f_{e0})^2$ in the E-μ phase space (δf_e is the electron density perturbation, and E and μ are the electron energy and magnetic moment, respectively). The initial δf_e is set to be zero, while the ion guiding center density perturbation is initiated as a flux-surface-averaged quantity. If trapped electron bounce motion resonates with GAM oscillation, the amplitude of $(\delta f_e/f_{e0})^2$ for the resonant electrons in the phase space will increase faster than the nonresonant electrons. As electron bounce frequency is only the function of E and μ, we plot the electron bounce frequency along with the $(\delta f_e/f_{e0})^2$ in the same E-μ phase space (Fig. 6). The electron bounce frequency is integrated by the following equation:

$$\omega_{be} = 2\pi/\tau_{be} = 2\pi\left(\int_{-\theta_b}^{\theta_b} \frac{dl}{|v_{\|}|}\right)^{-1} = 2\pi\left(\int_{-\theta_b}^{\theta_b} \frac{dl}{\sqrt{2(E-\mu B)}}\right)^{-1}. \quad (5)$$

Here τ_{be} and θ_b are the trapped electron bounce period and poloidal angle at the turning point, respectively. From figure we can see that the $(\delta f_e/f_{e0})^2$ of the trapped electrons with bounce frequency around the GAM frequency $\omega_{\mathrm{GAM}} = \omega_{be}$ is much larger than that of other trapped electrons. Comparing Figs. 6(a) and 6(b), we can see that the maximum of $(\delta f_e/f_{e0})^2$ locates at $E \approx 0.45(T_i)$ and $E \approx 1.0(T_i)$ for $q=4.0$ and $q=6.0$, respectively. It also agrees with the bounce frequency relation $\omega_{be} \propto \sqrt{T_i/q}$ for deeply trapped electrons. These simulation results clearly show that the enhancement of the GAM damping rate in simulations with kinetic electrons is due to the resonance between the GAM oscillation and the trapped electron bounce motion.

We now show that the passing electrons transit resonance is less important than the trapped electrons bounce resonance in the GAM collisionless damping. In the above simulations with $\epsilon=0.2$, electrons with $P > \sqrt{(1-\epsilon)/(1+\epsilon)} \approx 0.82$ are treated as kinetic electrons. Next, we fix $\epsilon=0.2$ and induce more passing electrons to be treated as kinetic electrons by decreasing the kinetic electrons simulation boundary from $P=0.82$ to $P=0.59$. In Fig. 7, as P changes from 0.82 to 0.59, the GAM amplitude only changes slightly. The results for $P=0.71$ and $P=0.59$ are almost identical,

which means if we further decrease P, the GAM damping rate would not change. Figure 8 is the $(\delta f_e/f_{e0})^2$ distribution in the simulation with $P=0.59$. The blue line corresponds to the kinetic electron boundary in the simulation, i.e., only electrons above the blue line in the E-μ space are treated as kinetic electrons in the simulation. The red line is the resonant transit frequency for passing electrons and we can clearly see a narrow colored contour line along the red line. This contour line shows the resonance of the passing electrons with the GAM oscillation. Comparing Figs. 8(a) and 8(b), we find that the passing electron resonance is stronger at $q=6$, which indicates that it is easier for passing electrons to resonate with the GAM at a larger q. It is obvious that most of the resonant passing electrons reside at $P>0.59$. This can provide an explanation on why the damping rate does not change if further decreasing P in Fig. 7. We can also see that the resonant contribution of the passing electrons is much smaller than that of the trapped electrons. This suggests that the trapped electrons effect is more important than the passing electrons in the GAM collisionless damping.

IV. CONCLUSION AND DISCUSSION

In this work, we use gyrokinetic particle simulation to study the zonal flow residual level and the GAM collisionless damping in the presence of kinetic electrons. Our simulation results of the residual level agree very well with the theory in appropriate limits. The kinetic electrons have little effects on the zonal flow residual level.

Our simulation results of the GAM frequency and collisionless damping rate with adiabatic electron response are also shown to correspond well with the theory. Comparisons between adiabatic electron response and kinetic electron response show that the GAM frequency is insensitive to the kinetic electrons but the GAM damping rate is greatly enhanced. Through the investigation of the perturbed electron distribution function in the phase space, we find that the enhancement of the GAM collisionless damping rate is due to the resonance of trapped electron bounce motion with the GAM oscillation. This result provides a possible explanation of the finite GAM damping rate in the high-q region of the tokamak edge, where the contribution of the ion resonance is small.

ACKNOWLEDGMENTS

One of the authors (H.S.Z.) acknowledges useful discussions with L. Chen, I. Holod, Z. Qiu, X. G. Wang, Y. Xiao, X. Q. Xu, and W. L. Zhang.

This work was supported by the U.S. Department of Energy (DOE), SciDAC GSEP, and GPS Centers, the China Scholarship Council (Grant No. 2009601135), the NSFC (Grant Nos. 40731056 and 10975012), and the National Basic Research Program of China (Grant Nos. 2008CB787103 and 2009GB105004).

[1] N. Winsor, J. L. Johnson, and J. J. Dawson, Phys. Fluids **11**, 2448 (1968).
[2] A. Hasegawa, C. G. Madennan, and Y. Kodama, Phys. Fluids **22**, 2122 (1979).
[3] A. V. Melnikov, V. A. Vershkov, L. G. Eliseev, S. A. Grashin, A. V. Gudozhnik, L. I. Krupnik, S. E. Lysenko, V. A. Mavrin, S. V. Perfilov, D. A. Shelukhin, S. V. Soldatov, M. V. Ufimtsev, A. O. Urazbaev, G. Van Oost, and L. G. Zimeleva, Plasma Phys. Controlled Fusion **48**, S87 (2006).
[4] T. Ido, Y. Miura, K. Kamiya, Y. Hamada, K. Hoshino, A. Fujisawa, K. Itoh, S. I. Itoh, A. Nishizawa, H. Ogawa, Y. Kusama, and JFT-2M Group, Plasma Phys. Controlled Fusion **48**, S41 (2006).
[5] A. Fujisawa, Nucl. Fusion **49**, 013001 (2009).
[6] G. R. McKee, D. K. Gupta, R. J. Fonck, D. J. Schlossberg, M. W. Shafer, and P. Gohil, Plasma Phys. Controlled Fusion **48**, S123 (2006).
[7] G. D. Conway, B. Scott, J. Schirmer, M. Reich, A. Kendl, and ASDEX Upgrade Team, Plasma Phys. Controlled Fusion **47**, 1165 (2005).
[8] K. J. Zhao, T. Lan, J. Q. Dong, L. W. Yan, W. Y. Hong, C. X. Yu, A. D. Liu, J. Qian, J. Cheng, D. L. Yu, Q. W. Yang, X. T. Ding, Y. Liu, and C. H. Pan, Phys. Rev. Lett. **96**, 255004 (2006).
[9] Z. Lin, T. S. Hahm, W. W. Lee, W. M. Thang, and R. B. White, Science **281**, 1835 (1998).
[10] K. Hallatschek and D. Biskamp, Phys. Rev. Lett. **86**, 1223 (2001).
[11] V. B. Lebedev, P. N. Yushmanov, P. H. Diamond, and S. V. Novakovskii, Phys. Plasmas **3**, 3023 (1996).
[12] S. V. Novakovskii, C. S. Liu, R. Z. Sagdeev, and M. N. Rosenbluth, Phys. Plasmas **4**, 4272 (1997).
[13] X. Q. Xu, Z. Xiong, Z. Gao, W. M. Nevins, and G. R. Mckee, Phys. Rev. Lett. **100**, 215001 (2008).
[14] Z. Gao, K. Itoh, H. Sanuki, and J. Q. Dong, Phys. Plasmas **15**, 072511 (2008).
[15] H. Sugama and T. H. Watanabe, J. Plasma Phys. **72**, 825 (2006).
[16] F. Zonca and L. Chen, Europhys. Lett. **83**, 35001 (2008).
[17] Y. Xiao, I. Holod, W. L. Zhang, S. Klasky, and Z. Lin, Phys. Plasmas **17**, 022302 (2010).
[18] G. Y. Fu, Phys. Rev. Lett. **101**, 185002 (2008).
[19] Y. Nagashima, K. Itoh, S.-I. Itoh, A. Fujisawa, M. Yagi, K. Hoshino, K. Shinohara, A. Ejiri, Y. Takase, T. Ido, K. Uehara, Y. Miura, and JFT-2M Group, Plasma Phys. Controlled Fusion **49**, 1611 (2007).
[20] R. Nazikian, private communication (2008).
[21] N. Chakrabarti, R. Singh, P. K. Kaw, and P. N. Guzdar, Phys. Plasmas **14**, 052308 (2007).
[22] M. Sasaki, K. Itoh, Y. Nagashima, A. Ejiri, and Y. Takase, Phys. Plasmas **16**, 022306 (2009).
[23] M. Sasaki, K. Itoh, A. Ejiri, and Y. Takase, Plasma Phys. Controlled Fusion **51**, 085002 (2009).
[24] A. B. Mikhailovskii, A. I. Smolyakov, A. P. Churikov, and V. D. Pustovitov, Plasma Phys. Controlled Fusion **51**, 075010 (2009).
[25] H. S. Zhang, Z. Qiu, L. Chen, and Z. Lin, Nucl. Fusion **49**, 125009 (2009).
[26] S. Satake, M. Okamoto, N. Nakajima, H. Sugama, M. Yokoyama, and C. D. Beidler, Nucl. Fusion **45**, 1362 (2005).
[27] Z. Qiu, L. Chen, and F. Zonca, Plasma Phys. Controlled Fusion **51**, 012001 (2009).
[28] X. Q. Xu, E. Belli, K. Bodi, J. Candy, C. S. Chang, R. H. Cohen, P. Colella, A. M. Dimits, M. R. Dorr, Z. Gao, J. A. Hittinger, S. Ko, S. Krasheninnikov, G. R. McKee, W. M. Nevins, T. D. Rognlien, P. B. Snyder, J. Suh, and M. V. Umansky, Nucl. Fusion **49**, 065023 (2009).
[29] I. Holod, W. L. Zhang, Y. Xiao, and Z. Lin, Phys. Plasmas **16**, 122307 (2009).
[30] M. N. Rosenbluth and F. L. Hinton, Phys. Rev. Lett. **80**, 724 (1998).
[31] Z. Lin, T. S. Hahm, W. W. Lee, W. M. Tang, and R. B. White, Phys. Plasmas **7**, 1857 (2000).
[32] Y. Xiao and P. J. Catto, Phys. Plasmas **13**, 082307 (2006).
[33] Z. Lin and L. Chen, Phys. Plasmas **8**, 1447 (2001).
[34] Z. Lin, Y. Nishimura, Y. Xiao, I. Holod, W. L. Zhang, and L. Chen, Plasma Phys. Controlled Fusion **49**, B163 (2007).